Instability analysis of spin-torque oscillator with an in-plane magnetized free layer and a perpendicularly magnetized pinned layer

Tomohiro Taniguchi and Hitoshi Kubota

Phys. Rev. B **93**, 174401 — Published 2 May 2016

DOI: 10.1103/PhysRevB.93.174401

Instability analysis of spin torque oscillator with an in-plane magnetized free layer and a perpendicularly magnetized pinned layer

Tomohiro Taniguchi and Hitoshi Kubota

National Institute of Advanced Industrial Science and Technology (AIST), Spintronics Research Center, Tsukuba, Ibaraki 305-8568, Japan

Abstract

We study the theoretical conditions to excite a stable self-oscillation in a spin torque oscillator with an in-plane magnetized free layer and a perpendicularly magnetized pinned layer in the presence of magnetic field pointing in an arbitrary direction. The linearized Landau-Lifshitz-Gilbert (LLG) equation is found to be inapplicable to evaluate the threshold between the stable and self-oscillation states because the critical current density estimated from the linearized equation is considerably larger than that found in the numerical simulation. We derive a theoretical formula of the threshold current density by focusing on the energy gain of the magnetization from the spin torque during a time shorter than a precession period. A good agreement between the derived formula and the numerical simulation is obtained. The condition to stabilize the out-of-plane self-oscillation above the threshold is also discussed.

PACS numbers: 75.78.Jp, 75.76.+j, 85.75.-d

I. INTRODUCTION

A spin polarized current injected into a nanostructured ferromagnet creates spin torque through the spin-transfer effect [1–3]. The spin torque provides rich variety of magnetization dynamics such as switching or self-oscillation [4–10]. In particular, a spin torque oscillator consisting of an in-plane magnetized free layer and a perpendicularly magnetized pinned layer has been an attractive research subject in the field of magnetism. [11–21]. In this type of spin torque oscillator, the spin torque forces the magnetization of the free layer into out of plane, and excites a large amplitude oscillation around the perpendicular axis. A high symmetry along the perpendicular direction in this system makes it easy to investigate the oscillation properties theoretically [17]. In order to observe the oscillation experimentally through magnetoresistance effect, however, the symmetry breaking should occur since the change of the relative angle between the magnetizations of the free and pinned layers in time is necessary. The linear analysis in the presence of an in-plane anisotropy [16] or the perturbation approach to the system additionally having an in-plane magnetized reference layer [19] have been made to develop practical theory.

The application of an external magnetic field tilted from the perpendicular axis also breaks the symmetry, and enables us to measure the oscillation experimentally. In other geometries, the experimental studies have shown that the oscillation properties such as the threshold current to excite the self-oscillation strongly depend on the field direction [6,10]. On the other hand, the role of the magnetic field on the self-oscillation properties in this geometry has not been fully understood yet. For example, it is still unclear how much current is necessary to excite the out-of-plane self-oscillation in the presence of the magnetic field pointing in an arbitrary direction, while it is known that infinitesimal current can excite the self-oscillation for highly symmetric case [12,17].

In this paper, we investigate theoretical conditions to excite the self-oscillation in a spin torque oscillator with an in-plane magnetized free layer and a perpendicularly magnetized pinned layer in the presence of an external magnetic field. We solve the Landau-Lifshitz-Gilbert (LLG) equation both numerically and analytically. The main findings in this paper are as follows. First, we find that the linearized LLG equation is no longer useful to evaluate the instability threshold in the present system. The critical current density evaluated from the linearized LLG equation is two orders of magnitude larger than the instability threshold

estimated from the numerical simulation. Second, we derive the theoretical formula determining the instability threshold. The main difference between the linear analysis and our result is that when a periodic precession around the stable state is assumed in the linear analysis, while we focus on the transition of the magnetization from the stable state to the out-of-plane self-oscillation state during a time shorter than the precession period. A good agreement between the numerical simulation and our formula is obtained. Third, we derive theoretical conditions to guarantee the present results, i.e., the condition that our formula of the threshold current density works better than the linear analysis to estimate the instability threshold, and the condition to stabilize the out-of-plane self-oscillation.

This paper is organized as follows. In Sec. II, we show the numerical simulation results near the instability of the initial state. We also solve the linearized LLG equation analytically. In Sec. III, we derive a theoretical formula of the threshold current, and confirm its validity by comparing the results obtained from the formula with the numerical simulation. The conclusion is summarized in Sec. IV.

II. NUMERICAL SIMULATION AND LINEAR ANALYSIS

In this section, we investigate the threshold current density which is necessary to destabilize the magnetization in the stable state by numerically solving the LLG equation. We also compare the numerical result with the analytical values of the critical current density j_c estimated from the linearized LLG equation. Throughout this paper, the term "threshold current" indicates the current destabilizing the stable state calculated in the numerical simulation or from the formula which is also well consistent with the numerical simulation, while the term "critical current" is a current estimated from the linearized LLG equation.

A. System description

The system we consider is schematically shown in Fig. 1(a). The z axis is perpendicular to the film plane. The unit vectors pointing in the magnetization direction of the free and pinned layers are denoted as $\mathbf{m}$ and $\mathbf{p}$, respectively. The magnetization of the pinned layer points to the positive z direction, $\mathbf{p} = +\mathbf{e}_z$. The positive current is defined as the electrons flowing from the free layer to the pinned layer. We use the macrospin approximation to the

free layer. The magnetization dynamics is described by the LLG equation

$$\frac{d\mathbf{m}}{dt} = -\gamma \mathbf{m} \times \mathbf{H} - \gamma H_{\rm s} \mathbf{m} \times (\mathbf{p} \times \mathbf{m}) + \alpha \mathbf{m} \times \frac{d\mathbf{m}}{dt}, \tag{1}$$

where γ and α are the gyromagnetic ratio and the Gilbert damping constant, respectively. We use the approximation $1+\alpha^2 \simeq 1$ because the damping constant for typical ferromagnets is on the order of $10^{-2} - 10^{-3}$ [22,23]. The spin torque strength is

$$H_{\rm s} = \frac{\hbar \eta j}{2eMd}, \tag{2}$$

where η is the spin polarization of the electric current density j, while M and d are the saturation magnetization and the thickness of the free layer, respectively. We neglect the asymmetry of the spin torque described by the term $1/(1 + \lambda \mathbf{m} \cdot \mathbf{p})$ [1] here, for simplicity. The critical current density in the presence of this factor, as well as its role, is briefly summarized in Appendix A. The magnetic field $\mathbf{H}$ consists of the demagnetization field along the z direction, $-4\pi M$, and the applied $\mathbf{H}_{\rm appl}$ expressed as

$$\mathbf{H} = \mathbf{H}_{\rm appl} - 4\pi M m_z \mathbf{e}_z. \tag{3}$$

The applied field, $\mathbf{H}_{\rm appl}$, is tilted from the z axis and assume to lie in xz plane for convention, i.e.,

$$\mathbf{H}_{\rm appl} = H_{\rm appl} \sin\theta_H \mathbf{e}_x + H_{\rm appl} \cos\theta_H \mathbf{e}_z, \tag{4}$$

where $H_{\rm appl}$ and θ_H are the amplitude and the tilted angle from the z axis of the applied field, respectively. The magnetic field relates to the energy density E via $E = -M \int d\mathbf{m} \cdot \mathbf{H}$, which in the present system is

$$E = -MH_{\rm appl} (\sin\theta_H m_x + \cos\theta_H m_z) + 2\pi M^2 m_z^2. \tag{5}$$

Here, we assume that $H_{\rm appl} < 4\pi M$, and therefore, the stable state, i.e., the minimum of Eq. (5), locates close to the x axis. Note that the magnetization dynamics described by Eq. (1) can be regarded as the motion of a point particle on an unit sphere.

The values of the parameters used in this section are brought from typical experiments [24], $M = 1300$ emu/c.c., $\gamma = 1.764 \times 10^7$ rad/(Oe s), $\alpha = 0.01$, $d = 2$ nm, and $\eta = 0.5$. The magnitude of the applied field is $H_{\rm appl} = 650$ Oe, while the field angle is $\theta_H = 5^\circ$. Figure 1(b) shows the constant energy curves of Eq. (5) with these parameters. Note that the

stable (minimum energy) state, the saddle point, and the unstable (local maximum) states of the energy density E all exist in the xz plane. The stable state locates in the positive x region, while the saddle point exists in the negative x region. Also, the unstable states slightly shift from the z axis due to the applied field. We denote the energies corresponding to the stable state, the saddle point, and the unstable states as $E_{\rm min}$, $E_{\rm saddle}$, and $E_{\rm max\pm}$, where the subscript $\pm$ distinguishes the unstable states in the positive (+) and negative ($-$) z region. For $\theta_H \neq 90^\circ$, $E_{\rm max+} \neq E_{\rm max-}$. The constant energy curves in Fig. 1(b) are classified to the ellipses around the x and z axes. The energy density E corresponding to the curves around the x axis is in the region of $E_{\rm min} \leq E \leq E_{\rm saddle}$, while that for the curves around the z axis is in the region of $E_{\rm saddle} < E \leq E_{\rm max\pm}$.

B. Linear analysis

The conventional method to estimate the minimum current density to destabilize the stable state is linearizing the LLG equation, and investigate the oscillating solution of the magnetization with a complex frequency [25–27]. In this section, we derive the theoretical formula of the critical current density, and estimate its value.

We introduce the zenith and azimuth angles (θ, φ) as $\mathbf{m} = (\sin\theta\cos\varphi, \sin\theta\sin\varphi, \cos\theta)$ to identify the magnetization direction. In particular, the angles corresponding to the stable state are denoted as (θ_0, φ_0). In the present case, $\varphi_0 = 0$, and θ_0 is determined by the condition $(\partial E/\partial\theta)_{\varphi=\varphi_0} = 0$,

$$H_{\rm appl}\sin(\theta_H - \theta_0) + 4\pi M \sin\theta_0\cos\theta_0 = 0. \tag{6}$$

We introduce a new coordinate XYZ where the Z axis is parallel to the magnetization in the stable state (θ_0, φ_0). A small amplitude oscillation of the magnetization around a stationary point is described by the following linearized LLG equation (the detail of the derivation is shown in Appendix A)

$$\frac{1}{\gamma}\frac{d}{dt}\begin{pmatrix} m_X \\ m_Y \end{pmatrix} + \mathsf{M}\begin{pmatrix} m_X \\ m_Y \end{pmatrix} = H_{\rm s}\begin{pmatrix} \sin\theta_0 \\ 0 \end{pmatrix}, \tag{7}$$

where

$$\mathsf{M} = \begin{pmatrix} \alpha H_X - H_{\rm s}\cos\theta_0 & H_Y \\ -H_X & \alpha H_Y - H_{\rm s}\cos\theta_0 \end{pmatrix} \tag{8}$$

with $H_X = H_{\rm appl}\cos(\theta_H - \theta_0) - 4\pi M \cos 2\theta_0$ and $H_Y = H_{\rm appl}\cos(\theta_H - \theta_0) - 4\pi M \cos^2\theta_0$. The solution of Eq. (7) has a form of $\exp\{\gamma[\pm i\sqrt{\det[\mathsf{M}] - (\mathrm{Tr}[\mathsf{M}/2])^2} - \mathrm{Tr}[\mathsf{M}]/2]t\}$. The critical current density is defined as the current density satisfying $\mathrm{Re}[\pm i\sqrt{\det[\mathsf{M}] - (\mathrm{Tr}[\mathsf{M}/2])^2} - \mathrm{Tr}[\mathsf{M}]/2] = 0$. For a small α, this condition is approximated to $\mathrm{Tr}[\mathsf{M}/2] = 0$ because $(\mathrm{Tr}[\mathsf{M}/2])^2/\det[\mathsf{M}] \sim \alpha^2 \simeq 0$. Therefore, the critical current density becomes

$$j_{\rm c} = \frac{2\alpha e M d}{\hbar\eta\cos\theta_0}\left[H_{\rm appl}\cos(\theta_H - \theta_0) - 4\pi M\frac{\cos^2\theta_0 + \cos 2\theta_0}{2}\right]. \tag{9}$$

Substituting the above parameters, we find that $\theta_0 \simeq 87.7^\circ$ and $j_{\rm c} = 328 \times 10^6 \mathrm{A/cm^2}$.

C. Numerical simulation

Figures 2(a)-(d) show the magnetization dynamics on the unit sphere and time developments of the components of **m**, obtained by numerically solving the LLG equation, Eq. (1). The current density is (a) 7.2, (b) 7.3, (c) -7.2, and (d) -7.3 $\times 10^6$ A/cm^2. As shown, when the current magnitude $|j|$ is smaller than 7.2×10^6 A/cm^2, the magnetization finally moves to another point and stops its dynamics. On the other hand, the magnetization shows the self-oscillation for $|j| \geq 7.3 \times 10^6 \mathrm{A/cm^2}$. The z component of the magnetization moves to the positive (negative) z direction for the negative (positive) current because the negative (positive) current prefers **m** to be parallel (antiparallel) to the magnetization of the pinned layer, $\mathbf{p} = +\mathbf{e}_z$.

Three important conclusions are obtained from Fig. 2. First, the threshold current density to destabilize the initial stable state, $\simeq \pm 7.3 \times 10^6$ A/cm^2, is two orders of magnitude smaller than the critical current density, $j_{\rm c} = 328 \times 10^6$ A/cm^2, estimated from the linearized LLG equation. Second, both positive and negative currents can destabilize the initial state, while the sign of $j_{\rm c}$ is fixed (positive for $\theta_H < 90^\circ$). Third, the magnetization precesses around the z axis above the threshold. Note that the self-oscillation occurs on the trajectory close to the constant energy curve. Although the energy landscape has the constant energy curves around the x axis, as shown in Fig. 1(b), an in-plane precession around the x axis does not appear. In the next section, we explain the physical meanings of such behavior.

III. THEORETICAL FORMULA OF THRESHOLD CURRENT

The results discussed in the previous section indicates that the linear analysis is no longer applicable to evaluate the instability threshold, although the linear analysis has been widely used to analyze the spin torque induced magnetization dynamics [25–27]. In this section, we clarify the reason for the breakdown of the linear analysis, and derive a theoretical formula of the threshold current density by focusing on the energy gain of the free layer generated from the work done by spin torque.

A. LLG equation averaged over constant energy curves

Here, let us discuss the averaging technique of the LLG equation on the constant energy curves. This method has been used in several works to analyze the self-oscillation and the thermally activated magnetization switching induced by spin torque, the microwave assisted magnetization reversal, and so on [28–40]. As will be discussed below, the critical current density $j_{\rm c}$ introduced above corresponds to a special limit of this averaging technique. Therefore, by reviewing the derivation of the averaged LLG equation, the reason why the linearized LLG equation does not work to estimate the instability condition accurately will be clarified.

The self-oscillation is a steady precession on a constant energy curve of E excited by the magnetic field torque $(-\gamma\mathbf{m}\times\mathbf{H})$. To maintain the precession, the spin torque should balance with the damping torque. Note however that the spin torque and the damping torque have different angular dependences. Therefore, strictly speaking, the spin torque may overcome the damping torque at certain points on the precession trajectory, the damping torque may however overcome the spin torque at other points. The self-oscillation is maintained when the shift from the constant energy curve due to the imbalance between the spin torque and the damping torque is sufficiently small. In that case, the magnetization can return back to the original constant energy curve during the precession. When this condition is satisfied, we obtain the following averaged LLG equation,

$$\oint dt\frac{dE}{dt} = \mathscr{W}_{\rm s}(E) + \mathscr{W}_{\alpha}(E), \tag{10}$$

where the integral range is a precession period on a constant energy curve of E. The work

done by spin torque and the dissipation due to the damping during the precession are

$$\mathscr{W}_{\rm s} = \oint dt\gamma M H_{\rm s} \left[\mathbf{p}\cdot\mathbf{H} - (\mathbf{m}\cdot\mathbf{p})\,(\mathbf{m}\cdot\mathbf{H})\right], \tag{11}$$

$$\mathscr{W}_{\alpha} = -\oint dt\alpha\gamma M \left[\mathbf{H}^2 - (\mathbf{m}\cdot\mathbf{H})^2\right], \tag{12}$$

respectively. Since the energy density averaged over the precession is conserved in the self-oscillation state, the self-oscillation is described by the equation $\oint dt(dE/dt) = 0$. Therefore, the current density necessary to excite a self-oscillation on a certain constant energy curve of E is

$$j(E) = \frac{2\alpha e M d}{\hbar\eta} \frac{\oint dt[\mathbf{H}^2 - (\mathbf{m}\cdot\mathbf{H})^2]}{\oint dt[\mathbf{p}\cdot\mathbf{H} - (\mathbf{m}\cdot\mathbf{p})(\mathbf{m}\cdot\mathbf{H})]}. \tag{13}$$

The explicit form of $j(E)$ for an arbitrary E is obtained, in principle, by substituting the solution of the precession trajectory on a constant energy curve, which is described by $d\mathbf{m}/dt = -\gamma\mathbf{m}\times\mathbf{H}$. However, the solution is hardly obtained because the equation is a nonlinear equation. Therefore, we evaluate the integrals in Eq. (13) numerically, except for special cases mentioned below (see also Appendix B). The technique to evaluate the integrals in Eq. (13) is shown, for example, in Ref. [38]. The damping constant α is assumed to be scalar in the above formulation. On the other hand, a tensor damping was proposed in Ref. [41]. The presence of the tensor damping was also suggested in the spin torque problem [42]. The effect of the tensor damping can be taken into account by replacing α in Eq. (12) with the tensor damping; see Appendix C of Ref. [38].

B. Derivation of threshold current

Note that the critical current density $j_{\rm c}$, Eq. (9), obtained from the linearized LLG equation relates to Eq. (13) via

$$j_{\rm c} = \lim_{E\to E_{\rm min}} j(E). \tag{14}$$

Therefore, the fact that the critical current density $j_{\rm c}$ is quite larger than the threshold current density found in the numerical simulation indicates the breakdown of applying averaged LLG equation.

An important assumption in the averaged LLG equation is that the magnitudes of the spin torque and the damping torque are sufficiently small. Thus, a shift of the magnetization from a constant energy curve due to the imbalance between these torques is also small.

However, this assumption is not satisfied in the present case. Figure 3 shows the trajectory of the magnetization dynamics obtained from the numerical simulation, where the current density $j = -7.3 \times 10^6$ A/cm^2 is the threshold value found in Fig. 2(d). We also show the constant energy curve including the saddle point $\mathbf{m}_\mathrm{d}$. We should remind the readers that there are two kinds of constant energy curves, as shown in Fig. 1(b), i.e., the curves around the x axis corresponding to $E_\mathrm{min} \leq E \leq E_\mathrm{saddle}$ and the curves around the z axis corresponding to $E_\mathrm{saddle} < E \leq E_\mathrm{max\pm}$. The constant energy curve of E_saddle separates these in-plane and out-of-plane regions. As shown in Fig. 3, while the magnetization moves from the initial state to a point close to the saddle point, the magnetization crosses the constant energy curves of E_saddle, and transfers from the in-plane region to the out-of-plane region. A periodic oscillation around the stable state (x axis) is not excited. This result is the evidence that the assumption used in Eq. (13), as well as Eq. (9), is broken. Therefore, the critical current density j_c does not work to estimate the instability of the magnetization around the stable state accurately.

The inapplicability of the linearized LLG equation also relates to the value of the damping constant α. Note that both the spin torque and the damping torque move the magnetization from a constant energy curve, by either supplying or dissipating the energy from the free layer. Therefore, the averaging technique of the LLG equation, as well as the linearization of the LLG equation, works well for low damping case. The fact that the linearized LLG equation could not be applied in the above numerical simulation indicates that the value of the damping constant in the present system is high and that the precession around the stable state is not stabilized. The range of the damping constant where the linearized LLG equation will be applicable is discussed in Sec. III C below.

Figure 3 suggests that the magnetization can climb up the energy barrier $E_\mathrm{saddle} - E_\mathrm{min}$ by absorbing energy due to the work done by the spin torque during a time shorter than a precession period around the stable state. Therefore, the threshold current density can be defined as a current density satisfying the following equation,

$$\int_{\mathbf{m}_\mathrm{min}}^{\mathbf{m}_\mathrm{d}} dt \frac{dE}{dt} = E_\mathrm{saddle} - E_\mathrm{min}, \tag{15}$$

where $\mathbf{m}_\mathrm{min}$ corresponds to the initial stable state. Strictly speaking, the exact solution of the LLG equation is necessary to evaluate the threshold current density from Eq. (15). However, the LLG equation is a nonlinear equation, and it is difficult to obtain the exact

solution. Instead, we approximate Eq. (15) as

$$\int_{\mathbf{m}_{\mathrm{d}\pm}}^{\mathbf{m}_{\mathrm{d}}} dt \frac{dE}{dt} \simeq E_{\mathrm{saddle}} - E_{\mathrm{min}}, \tag{16}$$

where $\mathbf{m}_{\mathrm{d}\pm}$ are the points on the constant energy curve of E_{saddle} and are located in the xz plane; see Fig. 3. We note that Eq. (15) is well approximated by Eq. (16) when $\mathbf{m}_{\mathrm{d}\pm}$ locate close to $\mathbf{m}_{\mathrm{min}}$, which means that $H_{\mathrm{appl}}/(4\pi M) \ll 1$. Note that the left hand side of Eq. (16) can be evaluated in a similarly to the manner calculating Eq. (13) because the integral range is on the constant energy curve. However, the integral range is limited to $[\mathbf{m}_{\mathrm{d}\pm}, \mathbf{m}_{\mathrm{d}}]$ in Eq. (16), while the range is over a periodic precession in Eq. (13). The values of the integrals for these different regions are, in general, different. Since the value of the integral in Eq. (16) is determined by the energy landscape, and the time-dependent solution of Eq. (1) is unnecessary, the integral in Eq. (16) is easily evaluated than that in Eq. (15) [31].

The current density satisfying Eq. (16) is given by

$$\begin{aligned} j_{\mathrm{th}\pm} =& \frac{2\alpha e M d}{\hbar\eta} \frac{\int_{\mathbf{m}_{\mathrm{d}\pm}}^{\mathbf{m}_{\mathrm{d}}} dt[\mathbf{H}^2 - (\mathbf{m}\cdot\mathbf{H})^2]}{\int_{\mathbf{m}_{\mathrm{d}\pm}}^{\mathbf{m}_{\mathrm{d}}} dt[\mathbf{p}\cdot\mathbf{H} - (\mathbf{m}\cdot\mathbf{p})(\mathbf{m}\cdot\mathbf{H})]} \\ &+ \frac{2ed}{\gamma\hbar\eta} \frac{E_{\mathrm{saddle}} - E_{\mathrm{min}}}{\int_{\mathbf{m}_{\mathrm{d}\pm}}^{\mathbf{m}_{\mathrm{d}}} dt[\mathbf{p}\cdot\mathbf{H} - (\mathbf{m}\cdot\mathbf{p})(\mathbf{m}\cdot\mathbf{H})]}. \end{aligned} \tag{17}$$

Equation (17) is the theoretical formula of the threshold current density, and is the main result in this paper. This equation provides the estimation of the threshold current density with high accuracy. For example, the values of $j_{\mathrm{th}\pm}$ with the parameters used in Fig. 2 are $j_{\mathrm{th}+} = -7.7 \times 10^6 \mathrm{A/cm^2}$ and $j_{\mathrm{th}-} = 7.6 \times 10^6 \mathrm{A/cm^2}$, which show good agreement with the numerical results in Fig. 2. These values are estimated for $\theta_H = 5^\circ$. Below, we show that the agreement between Eq. (17) and the numerical simulation is obtained also for different values of θ_H; see Fig. 5. Note that $|j_{\mathrm{th}+}| \neq |j_{\mathrm{th}-}|$ because the magnetic field pointing in the positive z direction breaks the symmetry between the magnetization dynamics moving to the positive and negative z directions, although the difference is small. We emphasize that Eq. (17) consists of two parts. One is proportional to α because this term arises from the energy dissipation due to the damping. The other is, on the other hand, independent of α but proportional to the energy barrier $E_{\mathrm{saddle}} - E_{\mathrm{min}}$.

Equation (17) can be simplified into a different form for $\theta_H = 90^\circ$ (see also Appendix C). In this case, $E_{\mathrm{saddle}} = MH_{\mathrm{appl}}$, $E_{\mathrm{min}} = -MH_{\mathrm{appl}}$, and $\mathbf{m}_{\mathrm{d}\pm} = (\sqrt{1 - z_{\mathrm{d}\pm}^2}, 0, z_{\mathrm{d}\pm})$ with

$z_{\mathrm{d}\pm} = \pm 2\sqrt{h(1-h)}$ and $h = H_{\mathrm{appl}}/(4\pi M)$. Then, we find that

$$\int_{\mathbf{m}_{\mathrm{d}\pm}}^{\mathbf{m}_{\mathrm{d}}} dt \left[\mathbf{p}\cdot\mathbf{H} - (\mathbf{m}\cdot\mathbf{p})(\mathbf{m}\cdot\mathbf{H})\right] = \mp\frac{\pi}{\gamma}(1-h)^2, \tag{18}$$

$$\begin{aligned}&\int_{\mathbf{m}_{\mathrm{d}\pm}}^{\mathbf{m}_{\mathrm{d}}} dt \left[\mathbf{H}^2 - (\mathbf{m}\cdot\mathbf{H})^2\right] \\ &= \frac{16\pi M}{3\gamma}\sqrt{h(1-h)}\left(3-5h+2h^2\right).\end{aligned} \tag{19}$$

Therefore, Eq. (17) becomes

$$\begin{aligned}j_{\mathrm{th}\pm}(\theta_H = 90^\circ) = \mp\, &\frac{2eM^2 d}{\hbar\eta} \\ &\times \left[\frac{16\alpha}{3}\sqrt{\frac{h}{1-h}}(3-2h) + \frac{8h}{(1-h)^2}\right].\end{aligned} \tag{20}$$

Note that $j_{\mathrm{th}\pm} \to 0$ in the limit of $h = H_{\mathrm{appl}}/(4\pi M) \to 0$, indicating that infinitesimal current can destabilize the stable state in the absence of the applied field.

We note that both the positive and negative currents can destabilize the stable state in our picture, contrary to j_{c} having a fixed sign (positive for $\theta_H < 90^\circ$). The physical meaning of this difference is as follows. Since the damping torque always dissipates energy from the free layer, positive energy should be supplied from the work done by spin torque to destabilize the stable state. In the derivation of j_{c}, a steady precession around the stable state is assumed. On the precession trajectory, the spin torque has a component antiparallel to the damping torque when $m_z \lesssim 0$ and has a component parallel to the damping torque when $m_z \gtrsim 0$, for a positive current. The spin torque supplies energy to the free layer in the former case, but dissipates energy from the free layer in the latter case. Note that the trajectory slightly shifts to the positive direction due to the magnetic field having the positive z component, i.e., the trajectory is not symmetric with respect to the xy plane. Then, the work done by spin torque during the precession becomes finite and positive. The spin torque overcomes the damping torque when the current density becomes larger than j_{c}. When the current direction is reversed, the work done by spin torque becomes negative, and thus, the spin torque cannot overcome the damping. As a result, the sign of j_{c} is positive. However, as emphasized above, a periodic precession around the easy axis assumed in the derivation of j_{c} is not excited in the present case. Instead, we focused on the magnetization dynamics from $\mathbf{m}_{\mathrm{d}\pm}$ to $\mathbf{m}_{\mathrm{d}}$. The work done by spin torque during $[\mathbf{m}_{\mathrm{d}-}, \mathbf{m}_{\mathrm{d}}]$ becomes positive when the current has the positive sign. Similarly, the work during $[\mathbf{m}_{\mathrm{d}+}, \mathbf{m}_{\mathrm{d}}]$ is positive when the

current sign is negative. Therefore, both the positive and negative currents can destabilize the stable state by compensating the damping torque. Note also that the magnetization crosses the constant energy curve of $E_{\rm saddle}$ during a time shorter than a precession period around the x axis. Therefore, an in-plane self-oscillation on a constant energy curve of $E_{\rm min} \leq E \leq E_{\rm saddle}$ around the x axis cannot be excited in the present case.

C. Applicability of the present theory

There are two characteristic current scales, $j_{\rm c}$ and $j_{\rm th\pm}$, related to the magnetization dynamics, as discussed above. These two currents are defined from different mechanisms of the instability of the stable state. The instability condition of a precession around the stable state gives $j_{\rm c}$. On the other hand, $j_{\rm th\pm}$ was derived by the condition that the energy gain by the spin torque during a time shorter than the precession period becomes larger than the energy barrier between the stable state and the saddle point. The initial state is destabilized when the current magnitude becomes larger than $\min[j_{\rm c}, j_{\rm th\pm}]$. For the present parameters, $j_{\rm th\pm}$ is smaller than $j_{\rm c}$, and therefore, $j_{\rm th\pm}$ determines the instability threshold. The condition that $j_{\rm th\pm}$ works well to estimate the instability of the stable state can be expressed as

$$\frac{j_{\rm th\pm}}{j_{\rm c}} < 1. \tag{21}$$

This is another important equation in this paper, guaranteeing the validity of our approach. Whether Eq. (21) is satisfied or not depends on the material parameters, as well as the applied field magnitude and angle. If Eq. (21) is unsatisfied, $j_{\rm c}$ determines the instability threshold, the magnetization moves to the out-of-plane region after the magnetization precesses around the in-plane axis.

Note that the first term on the right hand side of Eq. (17) is proportional to the damping constant α, while the second term is independent of α. On the other hand, Eq. (9) is proportional to α. Therefore, Eq. (21) is not satisfied when α becomes sufficiently small. When Eq. (21) is unsatisfied, $j_{\rm c}$ determines the instability of the stable state. Then, we can discuss the minimum value of α guaranteeing the applicability of Eq. (21) [37]. The value α which falls off from the condition in Eq. (21) for the parameters used in Fig. 2 is $\alpha < 1.7 \times 10^{-4}$. This value of α is at least one to two orders of magnitude smaller than the experimentally reported values for conventional ferromagnets used in spin torque oscillator,

such as CoFeB [22,23]. Therefore, we consider that $j_{\rm th\pm}$ determines the instability of the stable state for typical experiments.

D. In the presence of the angular dependence of the spin torque

When the applied field points to the in-plane direction, $\theta_H = 90^\circ$, the stable state corresponds to $\theta_0 = 90^\circ$, and the critical current density in Eq. (9) diverges. This is because the work done by spin torque during the precession around the stable state becomes zero. Therefore, Eq. (21) is always satisfied for $\theta_H = 90^\circ$.

The divergence of $j_{\rm c}$ appears at a different field angle when the angular dependence of the spin torque is taken into account, although this term is neglected in the above calculation, for simplicity. In this case, Eq. (2) is replaced by

$$H_{\rm s} = \frac{\hbar\eta j}{2e(1+\lambda\mathbf{m}\cdot\mathbf{p})Md}. \tag{22}$$

Then, the critical current density becomes

$$j_{\rm c} = \frac{2\alpha eMd}{\hbar\eta P(\theta_0)}\left[H_{\rm appl}\cos(\theta_H-\theta_0) - 4\pi M\frac{\cos^2\theta_0+\cos 2\theta_0}{2}\right], \tag{23}$$

where $P(\theta_0)$ is given by

$$P(\theta_0) = \frac{\cos\theta_0}{1+\lambda\cos\theta_0} + \frac{\lambda\sin^2\theta_0}{2(1+\lambda\cos\theta_0)^2}, \tag{24}$$

see Appendix A. The divergence of the critical current density, Eq. (23), occurs at the angle θ_0 satisfying $P(\theta_0) = 0$. In particular, when $\theta_H = 90^\circ$, Eqs. (23) becomes

$$j_{\rm c}(\theta_H = 90^\circ) = \frac{4\alpha eMd}{\hbar\eta\lambda}\left(H_{\rm appl} + 2\pi M\right). \tag{25}$$

On the other hand, Eq. (17) is generalized for finite λ as

$$\begin{aligned} j_{\rm th\pm} =& \frac{2\alpha eMd}{\hbar\eta}\frac{\int_{\mathbf{m}_{\rm d\pm}}^{\mathbf{m}_{\rm d}} dt[\mathbf{H}^2-(\mathbf{m}\cdot\mathbf{H})^2]}{\int_{\mathbf{m}_{\rm d\pm}}^{\mathbf{m}_{\rm d}} dt[\mathbf{p}\cdot\mathbf{H}-(\mathbf{m}\cdot\mathbf{p})(\mathbf{m}\cdot\mathbf{H})]/(1+\lambda\mathbf{m}\cdot\mathbf{p})} \\ &+ \frac{2ed}{\gamma\hbar\eta}\frac{E_{\rm saddle}-E_{\rm min}}{\int_{\mathbf{m}_{\rm d\pm}}^{\mathbf{m}_{\rm d}} dt[\mathbf{p}\cdot\mathbf{H}-(\mathbf{m}\cdot\mathbf{p})(\mathbf{m}\cdot\mathbf{H})]/(1+\lambda\mathbf{m}\cdot\mathbf{p})}. \end{aligned} \tag{26}$$

Equation (26) for $\theta_H = 90^\circ$ is

$$j_{\rm th\pm}(\theta_H = 90^\circ) = \mp\frac{2eMd}{\hbar\eta}4\pi M\frac{\mathcal{N}}{\mathcal{D}_\pm}, \tag{27}$$

where $\mathcal{N}$ and $\mathcal{D}_\pm$ are

$$\begin{aligned}\mathcal{N} =& 4\lambda^2\left[2\alpha(3-2h)(1-h)\sqrt{h(1-h)}+3h\right] \\ & \times\sqrt{1-4\lambda^2 h(1-h)}\end{aligned} \tag{28}$$

$$\begin{aligned}\mathcal{D}_\pm =& 3\left\{\sqrt{1-4\lambda^2 h(1-h)}\left[\pi\mp 4\lambda\sqrt{h(1-h)}\right]\right. \\ & \left.-2\left[1-2\lambda^2(1-h)\right]\cos^{-1}\left[\pm 2\lambda\sqrt{h(1-h)}\right]\right\},\end{aligned} \tag{29}$$

see Appendix B. In the presence of a finite λ, $|j_{\rm th+}| \neq |j_{\rm th-}|$ even for $\theta_H = 90^\circ$. Eq. (27) reproduces Eq. (20) in the limit of $\lambda \to 0$. The currents, $j_{\rm c}$ and $j_{\rm th\pm}$, in Eq. (21) should be replaced by Eqs. (23) and (26) in the presence of the angular dependence of the spin torque.

E. Validity of Eq. (17) and condition to excite out-of-plane self-oscillation

In this section, we confirm the validity of Eq. (17) for a wide range of θ_H by comparing with the numerical simulation of the LLG equation.

Before the comparison, we briefly discuss the definition of the threshold current density estimated from the numerical simulation. We emphasize that $j_{\rm th\pm}$ just determines the instability of the stable state, and does not guarantee the existence of the out-of-plane self-oscillation. The out-of-plane self-oscillation is excited when a condition,

$$\frac{j(E)}{j_{\rm th\pm}} > 1, \tag{30}$$

is satisfied [39], where the range of E is $E_{\rm saddle} < E \leq E_{\rm max\pm}$. Note that the reason why the out-of-plane self-oscillations appear in Figs. 2(b) and 2(d) is that there exists a certain E satisfying Eq. (30). On the other hand, when Eq. (30) is not satisfied for any value of E, the magnetization moves to the point close to $-(+)\mathbf{e}_z$ for a positive (negative) current above $j_{\rm th\pm}$ because the spin torque magnitude becomes sufficiently strong, and the magnetization eventually becomes parallel or antiparallel to the magnetization of the pinned layer, $\mathbf{p} = +\mathbf{e}_z$. Figure 4 shows an example of such dynamics, where $\theta_H = 20^\circ$ and the current density is close to the threshold value, $-27.3 \times 10^6 {\rm A/cm}^2$, for this θ_H. As shown, the magnetization finally becomes almost parallel to the z axis. Such magnetization dynamics was observed experimentally [14]. The threshold current density evaluated from the numerical simulation should be defined as the current density above which the magnetization shows a stable out-of-plane self-oscillation or the magnetization moves to the points close to $\pm\mathbf{e}_z$. The detail of

the method numerically defining the threshold current density is summarized in Appendix D.

We study the validity of Eq. (17) by comparing with the threshold current estimated by numerically solving Eq. (1) for several values of θ_H and $H_{\rm appl}$. The threshold current density estimated from the numerical simulation of the LLG equation is shown by dots in Fig. 5(a), where the magnetic field angle θ_H varies in the range of $0 < \theta_H \leq 90^\circ$ while the magnitude $H_{\rm appl}$ is fixed to 650 Oe. We also shows the value of $j_{\rm th\pm}$ evaluated from Eq. (17) by solid lines. We find a good agreement between the numerical and theoretical results, supporting the validity of Eq. (17). The comparison between the numerically evaluated instability threshold and the analytical formula, Eq. (20), for several values of the field magnitude $H_{\rm appl}$ is shown in Fig. 5(b), where the field angle is fixed to $\theta_H = 90^\circ$. The theoretical formula agrees with the numerical result when $H_{\rm appl}/(4\pi M) \ll 1$, while the numerical result becomes different with the theoretical formula for relatively large magnetic field. This is because the derivation of the theoretical formula, Eq. (17), assumes that $H_{\rm appl}/(4\pi M) \ll 1$, as mentioned below Eq. (16). The current magnitude above which the difference between the theoretical and numerical results appears is on the order of 10^8 A/cm^2, which is one to two orders of magnitude larger than the current magnitude used in typical experiments [14,18,21,24]. Therefore, we consider that the present formula works well to analyze experiments for wide range of the applied field angle and magnitude.

We notice that $j(E)$ is an increasing function of E for the out-of-plane self-oscillation when $\lambda = 0$, as in the zero field case [12,17]. Then, there is a certain E satisfying Eq. (30) if

$$\frac{j_{\rm u\pm}}{j_{\rm th\pm}} > 1, \tag{31}$$

is satisfied, where $j_{\rm u\pm}$ are Eq. (13) at the unstable states, $E = E_{\rm max\pm}$,

$$j_{\rm u\pm} \equiv \lim_{E \to E_{\rm max\pm}} j(E). \tag{32}$$

The dependences of $j_{\rm th\pm}$ and $j_{\rm u\pm}$ on the field angle θ_H and the magnitude $H_{\rm appl}$ are also shown in Figs. 5(a) and 5(b), respectively. It is shown that $j_{\rm u\pm}$ is almost independent of θ_H and $H_{\rm appl}$, while $j_{\rm th\pm}$ increases with increasing these parameters. For example, we find that $j_{\rm u\pm}/j_{\rm th\pm} > 1$ for $\theta_H < 20^\circ$. This result indicates that the out-of-plane self-oscillation can be excited for $\theta_H < 20^\circ$ for the present parameters. This finding is consistent with the numerical results shown in Figs. 2 and 4, supporting the validity of our argument. We notice that

the linearized LLG equation is useful to estimate $\lim_{E\to E_{\max\pm}} j(E)$ by replacing (θ_0, φ_0) with the zenith angle corresponding to the maximum point; see Eq. (A15). In particular, when $\theta_H = 90°$, the unstable states locate at $\mathbf{m}_{\rm u+} = (-H_{\rm appl}/(4\pi M), 0, \sqrt{1-[H_{\rm appl}/(4\pi M)]^2})$ and $\mathbf{m}_{\rm u-} = (-H_{\rm appl}/(4\pi M), 0, -\sqrt{1-[H_{\rm appl}/(4\pi M)]^2})$. Then, we find that (see also Appendix B)

$$j_{\rm u\pm}(\theta_H = 90°) = \mp\frac{2\alpha eMd}{\hbar\eta\sqrt{1-h^2}} 4\pi M \left(1 - \frac{h^2}{2}\right). \tag{33}$$

This equation indicates that $j_{\rm u\pm}(\theta_H = 90°) \simeq \mp[2\alpha eMd/(\hbar\eta)]4\pi M$ for $h \ll 1$, i.e., $j_{\rm u\pm}$ is almost independent of $H_{\rm appl}$, which is consistent with the result shown in Fig. 5(b).

IV. CONCLUSION

In conclusion, we studied the theoretical conditions to excite the self-oscillation in a spin torque oscillator consisting of an in-plane magnetized free layer and a perpendicularly magnetized pinned layer in the presence of an external magnetic field pointing in an arbitrary direction. The numerical simulation in Fig. 2 showed that the initial stable state is destabilized by current density much smaller than the critical current density estimated from the linearized LLG equation, Eq. (9). The fact implies that the linearized LLG equation is no longer applicable to evaluate the instability threshold in the present system. Then, we derived the theoretical formula of the threshold current density, Eq. (17), by focusing on the transition of the magnetization from the stable state to the out-of-plane precession during a time shorter than a precession period around the stable state. The derived formula consists of two parts, where one is proportional to the damping constant α, while the other is independent of α but proportional to the energy barrier $E_{\rm saddle} - E_{\rm min}$ for the transition. A good agreement between the numerical simulation and our formula, Eq. (17), is obtained in Fig. 5, indicating the validity of the formula. The condition that our formula of the threshold current density works better than the linear analysis to instability threshold is Eq. (21). We also derived the theoretical condition, Eq. (30), to stabilize the out-of-plane self-oscillation.

Acknowledgement

The authors express gratitude to Shinji Yuasa, Kay Yakushiji, Akio Fukushima, Shingo Tamaru, Sumito Tsunegi, Ryo Hiramatsu, Yoichi Shiota, Takehiko Yorozu, Hirofumi Suto, and Kiwamu Kudo for valuable discussion they had with us. This work is supported by Japan Society and Technology Agency (JST) strategic innovation promotion program "Development of new technologies for 3D magnetic recording architecture".

Appendix A: Derivation of linearized LLG equation

In this Appendix, we show the detail of the derivation of Eq. (7). For generality, we consider a ferromagnet having uniaxial anisotropies along the x, y, and z axes with an external magnetic field applied in an arbitrary direction. The magnetic field is given by

$$\mathbf{H} = \begin{pmatrix} H_{\rm appl}\sin\theta_H\cos\varphi_H - 4\pi M\tilde{N}_x m_x \\ H_{\rm appl}\sin\theta_H\sin\varphi_H - 4\pi M\tilde{N}_y m_y \\ H_{\rm appl}\cos\theta_H - 4\pi M\tilde{N}_z m_z \end{pmatrix}. \tag{A1}$$

The generalized demagnetization coefficient $\tilde{N}_i$ $(i = x, y, z)$ is defined as $4\pi M\tilde{N}_i = 4\pi MN_i - H_{{\rm K}i}$, where $4\pi MN_i$ is the shape anisotropy (demagnetization) field with $N_x + N_y + N_z = 1$, while $H_{{\rm K}i}$ is the crystalline or interface anisotropy field. The energy density $E = -M\int d\mathbf{m}\cdot\mathbf{H}$ is

$$\begin{aligned}\frac{E}{M} =& -H_{\rm appl}\left[\sin\theta_H\sin\theta\cos(\varphi_H-\varphi)+\cos\theta_H\cos\theta\right] \\ &+ 2\pi M\tilde{N}_x\sin^2\theta\cos^2\varphi + 2\pi M\tilde{N}_y\sin^2\theta\sin^2\varphi \\ &+ 2\pi M\tilde{N}_z\cos^2\theta.\end{aligned} \tag{A2}$$

The system in the main text corresponds to the case of $\tilde{N}_x = \tilde{N}_y = 0$, $\tilde{N}_z = 1$, and $\varphi_H = 0$.

Since we are interested in a small oscillation of the magnetization around the stable state, the zenith and azimuth angles corresponding to the stable state should be identified. The stable state is determined by the conditions that $\partial E/\partial\theta = \partial E/\partial\varphi = 0$, which are explicitly given by

$$\begin{aligned}&H_{\rm appl}\left[\sin\theta_H\cos\theta\cos(\varphi_H-\varphi)-\cos\theta_H\sin\theta\right] \\ &- 4\pi M\tilde{N}_x\sin\theta\cos\theta\cos^2\varphi - 4\pi M\tilde{N}_y\sin\theta\cos\theta\sin^2\varphi \\ &+ 4\pi M\tilde{N}_z\sin\theta\cos\theta = 0,\end{aligned} \tag{A3}$$

$$
\begin{aligned}
&H_{\rm appl}\sin\theta_H\sin\theta\sin(\varphi_H-\varphi)\\
&+4\pi M\tilde{N}_x\sin^2\theta\sin\varphi\cos\varphi-4\pi M\tilde{N}_y\sin^2\theta\sin\varphi\cos\varphi=0.
\end{aligned}
\tag{A4}
$$

Let us denote the zenith and azimuth angles satisfying Eqs. (A3) and (A4) as (θ_0,φ_0). As mentioned in the main text, we introduce the XYZ coordinate where the Z axis is parallel to the stable state (θ_0,φ_0). The rotation to the xyz coordinate to the XYZ coordinate is described by the rotation matrix

$$
\mathsf{R}=\begin{pmatrix}\cos\theta_0 & 0 & -\sin\theta_0\\ 0 & 1 & 0\\ \sin\theta_0 & 0 & \cos\theta_0\end{pmatrix}\begin{pmatrix}\cos\varphi_0 & \sin\varphi_0 & 0\\ -\sin\varphi_0 & \cos\varphi_0 & 0\\ 0 & 0 & 1\end{pmatrix}. \tag{A5}
$$

The relations between the components of $\mathbf{m}$ in the xyz and XYZ coordinates are $m_x=m_X\cos\theta_0\cos\varphi_0-m_Y\sin\varphi_0+m_Z\sin\theta_0\cos\varphi_0$, $m_y=m_X\cos\theta_0\sin\varphi_0+m_Y\cos\varphi_0+m_Z\sin\theta_0\sin\varphi_0$, $m_z=-m_X\sin\theta_0+m_Z\cos\theta_0$. Also, the magnetic field in the XYZ coordinate is

$$
\mathbf{H}=\begin{pmatrix}H_{XX}m_X+H_{XY}m_Y\\ H_{YX}m_X+H_{YY}m_Y\\ H_{ZX}m_X+H_{ZY}m_Y+H_{ZZ}\end{pmatrix}, \tag{A6}
$$

where

$$
\begin{aligned}
H_{XX}=&-4\pi M\tilde{N}_x\cos^2\theta_0\cos^2\varphi_0-4\pi M\tilde{N}_y\cos^2\theta_0\sin^2\varphi_0\\
&-4\pi M\tilde{N}_z\sin^2\theta_0,
\end{aligned}
\tag{A7}
$$

$$
H_{XY}=H_{YX}=-4\pi M\left(\tilde{N}_y-\tilde{N}_x\right)\cos\theta_0\sin\varphi_0\cos\varphi_0, \tag{A8}
$$

$$
H_{YY}=-4\pi M\tilde{N}_x\sin^2\varphi_0-4\pi M\tilde{N}_y\cos^2\varphi_0, \tag{A9}
$$

$$
\begin{aligned}
H_{ZX}=&-4\pi M\tilde{N}_x\sin\theta_0\cos\theta_0\cos^2\varphi_0\\
&-4\pi M\tilde{N}_y\sin\theta_0\cos\theta_0\sin^2\varphi_0\\
&+4\pi M\tilde{N}_z\sin\theta_0\cos\theta_0,
\end{aligned}
\tag{A10}
$$

$$
H_{ZY}=-4\pi M\left(\tilde{N}_y-\tilde{N}_x\right)\sin\theta_0\sin\varphi_0\cos\varphi_0, \tag{A11}
$$

$$
\begin{aligned}
H_{ZZ}=&H_{\rm appl}\left[\sin\theta_H\sin\theta_0\cos(\varphi_H-\varphi_0)+\cos\theta_H\cos\theta_0\right]\\
&-4\pi M\tilde{N}_x\sin^2\theta_0\cos^2\varphi_0-4\pi M\tilde{N}_y\sin^2\theta_0\sin^2\varphi_0\\
&-4\pi M\tilde{N}_z\cos^2\theta_0.
\end{aligned}
\tag{A12}
$$

Similarly, the magnetization of the pinned layer $\mathbf{p} = (p_x, p_y, p_z) = (\sin\theta_{\rm p}\cos\varphi_{\rm p}, \sin\theta_{\rm p}\sin\varphi_{\rm p}, \cos\theta_{\rm p})$ in the xyz coordinate transforms in the XYZ coordinate to

$$\mathbf{p} \equiv \begin{pmatrix} p_X \\ p_Y \\ p_Z \end{pmatrix} = \begin{pmatrix} \sin\theta_{\rm p}\cos\theta_0\cos(\varphi_{\rm p}-\varphi_0) - \cos\theta_{\rm p}\sin\theta_0 \\ \sin\theta_{\rm p}\sin(\varphi_{\rm p}-\varphi_0) \\ \sin\theta_{\rm p}\sin\theta_0\cos(\varphi_{\rm p}-\varphi_0) + \cos\theta_{\rm p}\cos\theta_0 \end{pmatrix}. \tag{A13}$$

Now we consider a small oscillation of the magnetization around the stable state. Using the approximations $m_Z \simeq 1$ and $|m_X|, |m_Y| \ll 1$, the LLG equation is linearized as

$$\begin{aligned} &\frac{1}{\gamma}\frac{d}{dt}\begin{pmatrix} m_X \\ m_Y \end{pmatrix} \\ &+ \begin{pmatrix} -H_{YX} - H_{\rm s}p_Z + \alpha H_X & H_Y - \alpha H_{XY} \\ -H_X - \alpha H_{YX} & H_{XY} - H_{\rm s}p_Z + \alpha H_Y \end{pmatrix}\begin{pmatrix} m_X \\ m_Y \end{pmatrix} \\ &= -H_{\rm s}\begin{pmatrix} p_X \\ p_Y \end{pmatrix}, \end{aligned} \tag{A14}$$

where $H_X = H_{ZZ} - H_{XX}$ and $H_Y = H_{ZZ} - H_{YY}$. The terms proportional to $\alpha H_{\rm s}$ are neglected because these terms are on the order of α^2. The condition that the trace of the coefficient matrix is zero gives

$$j_{\rm c} = \frac{2\alpha e M d}{\hbar\eta p_Z}\left(\frac{H_X + H_Y}{2}\right). \tag{A15}$$

Substituting $\tilde{N}_x = \tilde{N}_y = 0$, $\tilde{N}_z = 1$, $\varphi_H = 0$, and $\theta_{\rm p} = 0$, Eq. (A15) reproduces Eq. (9). On the other hand, in the case of the in-plane magnetized system considered in Ref. [26], i.e., $4\pi M\tilde{N}_x = -H_{\rm K}$, $\tilde{N}_y = 0$, $\tilde{N}_z = 1$, $\theta_H = 90^\circ$, $\varphi_H = 0$, $\theta_{\rm p} = 90^\circ$, and $\varphi_{\rm p} = 0$, we find that $H_{XX} = -4\pi M$, $H_{YY} = 0$, and $H_{ZZ} = H_{\rm appl} + H_{\rm K}$, where $H_{\rm K}$ is the in-plane anisotropy. Then, the critical current density becomes $j_{\rm c} = [2\alpha e M d/(\hbar\eta)](H_{\rm appl} + H_{\rm K} + 2\pi M)$, which is consistent with the result in Ref. [26].

The angular dependence of the spin torque, characterized by the factor $1/(1+\lambda\mathbf{m}\cdot\mathbf{p})$, can be taken into account as follows. As mentioned in the main text, $H_{\rm s}$ in this case is given by Eq. (22). In this case, Eq. (2) is replaced by Eq. (22). The factor $1/(1+\lambda\mathbf{m}\cdot\mathbf{p})$ is linearized as

$$\begin{aligned} \frac{1}{1+\lambda\mathbf{m}\cdot\mathbf{p}} &= \frac{1}{1+\lambda m_Z p_Z}\frac{1}{1+\frac{\lambda(m_X p_X + m_Y p_Y)}{1+\lambda m_Z p_Z}} \\ &\simeq \frac{1}{1+\lambda p_Z}\left[1 - \frac{\lambda(m_X p_X + m_Y p_Y)}{1+\lambda p_Z}\right]. \end{aligned} \tag{A16}$$

We introduce the following notations,

$$H_{\rm s}^{(0)} = \frac{\hbar\eta j}{2e(1+\lambda p_Z)Md}, \tag{A17}$$

$$\Lambda = \frac{\lambda}{1+\lambda p_Z}. \tag{A18}$$

Then, Eq. (A14) becomes

$$\frac{1}{\gamma}\frac{d}{dt}\begin{pmatrix} m_X \\ m_Y \end{pmatrix} + \mathsf{M}\begin{pmatrix} m_X \\ m_Y \end{pmatrix} = -H_{\rm s}^{(0)}\begin{pmatrix} p_X \\ p_Y \end{pmatrix}, \tag{A19}$$

where the components of the 2×2 matrix M are

$$\mathsf{M}_{1,1} = -H_{YX} - H_{\rm s}^{(0)}\left(p_Z + \Lambda p_X^2\right) + \alpha H_X, \tag{A20}$$

$$\mathsf{M}_{1,2} = H_Y - H_{\rm s}^{(0)}\Lambda p_X p_Y - \alpha H_{XY}, \tag{A21}$$

$$\mathsf{M}_{2,1} = -H_X - H_{\rm s}^{(0)}\Lambda p_X p_Y - \alpha H_{YX}, \tag{A22}$$

$$\mathsf{M}_{2,2} = H_{XY} - H_{\rm s}^{(0)}\left(p_Z + \Lambda p_Y^2\right) + \alpha H_Y. \tag{A23}$$

Then, the critical current determined by the condition $\mathrm{Tr}[\mathsf{M}] = 0$ is

$$j_{\rm c} = \frac{2\alpha e(1+\lambda p_Z)Md}{\hbar\eta[p_Z + \frac{\Lambda(1-p_Z^2)}{2}]}\left(\frac{H_X + H_Y}{2}\right). \tag{A24}$$

Equation (23) is obtained from Eq. (A24) by substituting $\tilde{N}_x = \tilde{N}_y = 0$, $\tilde{N}_z = 1$, $\varphi_H = 0$, and $\theta_{\rm p} = 0$,

Appendix B: Derivations of Eqs. (27) and (33)

Let us show the derivation of Eq. (33). As mentioned in the main text, $j_{\rm u\pm}$ can be obtained from the linearized LLG equation. Here, we show that $j_{\rm u\pm}$ can also be obtained as $j_{\rm u\pm} = \lim_{E\to E_{\rm max\pm}} j(E)$. This method provides an example of the calculation of Eq. (13).

Note that the maximum energies located at $\mathbf{m} \simeq \pm\mathbf{e}_z$, $E_{\rm max+} = E_{\rm max-}$, are identical for $\theta_H = 90^\circ$, and the corresponding energy density is $E_{\rm max} = (4\pi M^2/2)(1+h^2)$. Then, let us investigate $\lim_{E\to E_{\rm max}} j(E)$. Equation (13) can be rewritten as

$$j(E) = \frac{2\alpha eMd}{\hbar\eta}\frac{\mathscr{N}_\alpha}{\mathscr{N}_{\rm s}}, \tag{B1}$$

where $\mathscr{N}_{\rm s}$ and $\mathscr{N}_\alpha$ are, respectively, given by

$$\begin{aligned}\mathscr{N}_{\rm s} &= \gamma \int dt \left[\mathbf{p}\cdot\mathbf{H} - (\mathbf{m}\cdot\mathbf{p})(\mathbf{m}\cdot\mathbf{H})\right] \\ &= -\frac{1}{h}\int \frac{dm_z}{m_y}\left[m_z + \left(hm_x - m_z^2\right)m_z\right] \\ &= \int dm_z \frac{m_z^3 - 2(1-\epsilon)m_z}{\sqrt{(a-m_z^2)(m_z^2-b)}},\end{aligned} \tag{B2}$$

$$\begin{aligned}\mathscr{N}_\alpha &= \gamma \int dt \left[\mathbf{H}^2 - (\mathbf{m}\cdot\mathbf{H})^2\right] \\ &= (4\pi M)^2\gamma \int dt \left[h^2 + m_z^2 - \left(hm_x - m_z^2\right)^2\right] \\ &= -2\pi M \int dm_z \frac{m_z^4 - 4(1-\epsilon)m_z^2 + 4(\epsilon^2 - h^2)}{\sqrt{(a-m_z^2)(m_z^2-b)}}.\end{aligned} \tag{B3}$$

Here, we use the relation $dm_z/dt = \gamma H_{\rm appl} m_y$ obtained from the LLG equation on a constant energy curve, $d\mathbf{m}/dt = -\gamma\mathbf{m}\times\mathbf{H}$, with $\theta_H = 90^\circ$ [38]. The integral ranges of these integrals are discussed below. Equations (11) and (12) relate to Eqs. (B2) and (B3) via $\mathscr{W}_{\rm s} = 2MH_{\rm s}\mathscr{N}_{\rm s}$ and $\mathscr{W}_\alpha = -2\alpha M\mathscr{N}_\alpha$, where the numerical factor 2 appears by restricting the integral regions for $m_y > 0$, according to the symmetry [38]. The parameters a and b are given by

$$a = 2\left(\epsilon - h^2 + h\sqrt{1+h^2-2\epsilon}\right), \tag{B4}$$

$$b = 2\left(\epsilon - h^2 - h\sqrt{1+h^2-2\epsilon}\right), \tag{B5}$$

where $\epsilon = E/(4\pi M^2)$ is the normalized energy density. The physical meanings of a and b are as follows. Figure 6 shows the examples of the out-of-plane precession trajectories (constant energy curves) in the regions of $m_z > 0$ and $m_z < 0$. The precession directions are indicated by the arrows. The constant energies curves cross the xz plane at the points $m_z = \pm\sqrt{a}, \pm\sqrt{b}$. When we focus on the out-of-plane precession for $m_z > 0$, the integral ranges of Eqs. (B2) and (B3) are $\sqrt{b} \le m_z \le \sqrt{a}$. On the other hand, for the out-of-plane precession for $m_z < 0$, the integral range is $-\sqrt{a} \le m_z \le -\sqrt{b}$. Below, we calculate Eqs. (B2) and (B3) for $m_z < 0$. For $m_z > 0$, the sign of $\mathscr{N}_{\rm s}$ is changed.

We notice that Eqs. (B2) and (B3) are expressed as $\mathscr{N}_{\rm s} = I_3 - 2(1-\epsilon)I_1$ and $\mathscr{N}_\alpha = -2\pi M[I_4 - 4(1-\epsilon)I_2 + 4(\epsilon^2-h^2)I_0]$, respectively, where I_n $(n = 0, 1, 2, 3, 4)$ is

$$\begin{aligned}I_n &= \int_{-\sqrt{a}}^{-\sqrt{b}} dz \frac{z^n}{\sqrt{(a-z^2)(z^2-b)}} \\ &= \int_0^1 ds \frac{(-\sqrt{a}\sqrt{1-k^2s^2})^n}{\sqrt{a}\sqrt{(1-s^2)(1-k^2s^2)}}.\end{aligned} \tag{B6}$$

The modulus k is

$$k = \sqrt{1 - \frac{b}{a}}. \tag{B7}$$

The following formulas are useful to calculate $\mathscr{N}_{\rm s}$ and $\mathscr{N}_\alpha$;

$$I_0 = \frac{1}{\sqrt{a}} \int_0^1 \frac{ds}{\sqrt{(1-s^2)(1-k^2s^2)}} = \frac{1}{\sqrt{a}} \mathsf{K}(k), \tag{B8}$$

$$I_1 = -\int_0^1 \frac{ds}{\sqrt{1-s^2}} = -\frac{\pi}{2}, \tag{B9}$$

$$I_2 = \sqrt{a} \int_0^1 ds \sqrt{\frac{1-k^2s^2}{1-s^2}} = \sqrt{a} \mathsf{E}(k), \tag{B10}$$

$$I_3 = -a \int_0^1 ds \frac{1-k^2s^2}{\sqrt{1-s^2}} = -\frac{\pi a}{2} \left(1 - \frac{k^2}{2} \right), \tag{B11}$$

$$\begin{aligned} I_4 &= a^{3/2} \int_0^1 ds \sqrt{\frac{(1-k^2s^2)^3}{1-s^2}} \\ &= -\frac{a^{3/2}}{3} \left[(1-k^2)\mathsf{K}(k) - 2(2-k^2)\mathsf{E}(k) \right], \end{aligned} \tag{B12}$$

where $\mathsf{K}(k)$ and $\mathsf{E}(k)$ are the first and second kinds of complete elliptic integral. Substituting these formulas into Eqs. (B2) and (B3), Eq. (B1) becomes

$$\begin{aligned} j(E) = &-\frac{16\alpha e M^2 d}{3\hbar\eta} \times \\ &\frac{[-a^2(1-k^2) + 12(\epsilon^2 - h^2)]\mathsf{K}(k) + 2a[a(2-k^2) - 6(1-\epsilon)]\mathsf{E}(k)}{\sqrt{a}[4(1-\epsilon) - a(2-k^2)]}. \end{aligned} \tag{B13}$$

In the limit of $E \to E_{\rm max}$ ($\epsilon \to (1+h^2)/2$), Eq. (B13) gives $j_{\rm u-}$ in Eq. (33). By changing the integral range, as mentioned above, $j_{\rm u+}$ is also obtained.

Equation (27) is obtained in a similar manner. Equations (B2) and (B3) can be used to evaluate the integrals in Eq. (26). Note that the integral range to derive Eq. (33) is over an out-of-plane precession trajectory, while the range in Eq. (26) is $[\mathbf{m}_{\rm d\pm}, \mathbf{m}_{\rm d}]$. We notice that a and b in Eqs. (B2) and (B3) are $4h(1-h)$ and $b = 0$ on the constant energy curve including the saddle point because $E_{\rm saddle} = MH_{\rm appl}$ ($\epsilon = h$). Then, Eqs. (B2) and (B3) for $j_{\rm th\pm}$ are given by

$$\mathscr{N}_{\rm s}^{\pm} = \mp \int dm_z \frac{m_z^2 - 2(1-h)}{(1+\lambda m_z)\sqrt{4h(1-h) - m_z^2}}, \tag{B14}$$

$$\mathscr{N}_\alpha^{\pm} = \pm 2\pi M \int dm_z \frac{[m_z^2 - 4(1-h)]m_z}{\sqrt{4h(1-h) - m_z^2}}. \tag{B15}$$

The integral range is $[2\sqrt{h(1-h)}, 0]$ for $j_{\rm th+}$ and $[-2h\sqrt{h(1-h)}, 0]$ for $j_{\rm th-}$. We notice that $\mathscr{N}_{\rm s}^{\pm} = \mp[J_2' - 2(1-h)J_0']_{\pm 2\sqrt{h(1-h)}}^{0}$ and $\mathscr{N}_{\alpha}^{\pm} = \pm 2\pi M[J_3 - 4(1-h)J_1]_{\pm\sqrt{2h(1-h)}}^{0}$, where

$$J_n = \int dz \frac{z^n}{\sqrt{a-z^2}}, \tag{B16}$$

$$J_n' = \int dz \frac{z^n}{(1+\lambda z)\sqrt{a-z^2}}. \tag{B17}$$

Moreover, these integrals satisfy $J_2' = (J_0' - J_0)/\lambda^2 + (J_1/\lambda)$. Then, using the following formulas, Eq. (27) is obtained;

$$J_0 = \int \frac{dz}{\sqrt{a-z^2}} = \sin^{-1}\left(\frac{z}{\sqrt{a}}\right), \tag{B18}$$

$$J_1 = \int dz \frac{z}{\sqrt{a-z^2}} = -\sqrt{a-z^2}, \tag{B19}$$

$$J_3 = \int dz \frac{z^3}{\sqrt{a-z^2}} = -\frac{\sqrt{a-z^2}(2a+z^2)}{3}, \tag{B20}$$

$$J_0' = \int \frac{dz}{(1+\lambda z)\sqrt{a-z^2}} = \frac{1}{\sqrt{1-\lambda^2 a}} \sin^{-1}\left[\frac{z+\lambda a}{\sqrt{a}(1+\lambda z)}\right]. \tag{B21}$$

Appendix C: Instability condition in terms of magnetic field

In the main text, we derive the threshold current density as a function of the magnetic field. In some experiments [18,21,24], on the other hand, the instability threshold is investigated by fixing the value of the applied current (voltage) and changing the magnetic field magnitude. The threshold magnetic field magnitude below which the self-oscillation is excited was found experimentally [24], which indicates that the threshold magnetic field is a decreasing function of θ_H ($0 < \theta_H \leq 90^\circ$). The theoretical formula of the threshold magnetic field, $H_{\rm th}$, is, in principle, obtained by rewriting the instability threshold condition, Eq. (17), in terms of the magnetic field. For example, when $\theta_H = 90^\circ$ and $H_{\rm appl}/(4\pi M) \ll 1$, Eq. (20) is rewritten as

$$H_{\rm th}(\theta_H = 90^\circ) \simeq 4\pi M \left(\frac{\hbar\eta|j|}{16eM^2d} - \alpha\sqrt{\frac{\hbar\eta|j|}{4eM^2d} + 4\alpha^2} + 2\alpha^2 \right). \tag{C1}$$

Although it is difficult to derive analytical formula of the threshold magnetic field for an arbitary value of θ_H because the right hand side of Eq. (17) is a complex function of the magnetic field, the experimental result [24] indicates that $H_{\rm th}(\theta_H)\sin\theta_H \simeq H_{\rm th}(\theta_H = 90^\circ)$.

Appendix D: Definition of the threshold current density in numerical simulation

We solve the LLG equation numerically from $t = 0$ to $t = 20$ ns by using the fourth-order Runge-Kutta method. The time step is $\Delta t = 10$ fs. The threshold current density in the numerical simulation is defined as a minimum current density satisfying $|m_x(t = 20\text{ns}) - m_x(t = 20\text{ns} - \Delta t)| > 10^{-10}$ or $|m_z(t = 20\text{ns})| > 0.9$, where the former means that the magnetization is in the oscillating state while the latter means that the magnetization moves to $\pm\mathbf{e}_z$ direction.

---

[1] J. C. Slonczewski, J. Magn. Magn. Mater. **159**, L1 (1996).

[2] L. Berger, Phys. Rev. B **54**, 9353 (1996).

[3] J. C. Slonczewski, Phys. Rev. B **71**, 024411 (2005).

[4] J. A. Katine, F. J. Albert, R. A. Buhrman, E. B. Myers, and D. C. Ralph, Phys. Rev. Lett. **84**, 3149 (2000).

[5] S. I. Kiselev, J. C. Sankey, I. N. Krivorotov, N. C. Emley, R. J. Schoelkopf, R. A. Buhrman, and D. C. Ralph, Nature **425**, 380 (2003).

[6] W. H. Rippard, M. R. Pufall, S. Kaka, T. J. Silva, and S. E. Russek, Phys. Rev. B **70**, 100406 (2004).

[7] H. Kubota, A. Fukushima, Y. Ootani, S. Yuasa, K. Ando, H. Maehara, K. Tsunekawa, D. D. Djayaprawira, N. Watanabe, and Y. Suzuki, Jpn. J. Appl. Phys. **44**, L1237 (2005).

[8] I. N. Krivorotov, N. C. Emley, J. C. Sankey, S. I. Kiselev, D. C. Ralph, and R. A. Buhrman, Science **307**, 228 (2005).

[9] H. Kubota, K. Yakushiji, A. Fukushima, S. Tamaru, M. Konoto, T. Nozaki, S. Ishibashi, T. Saruya, S. Yuasa, T. Taniguchi, et al., Appl. Phys. Express **6**, 103003 (2013).

[10] S. Tamaru, H. Kubota, K. Yakushiji, T. Nozaki, M. Konoto, A. Fukushima, H. Imamura, T. Taniguchi, H. Arai, T. Yamaji, et al., Appl. Phys. Express **7**, 063005 (2014).

[11] A. D. Kent, B. Özyilmaz, and E. del Barco, Appl. Phys. Lett. **84**, 3894 (2004).

[12] K. J. Lee, O. Redon, and B. Dieny, Appl. Phys. Lett. **86**, 022505 (2005).

[13] X. Zhu and J.-G. Zhu, IEEE Trans. Magn. **42**, 2670 (2006).

[14] D. Houssameddine, U. Ebels, B. Delaët, B. Rodmacq, I. Firastrau, F. Ponthenier, M. Brunet,

C. Thirion, J.-P. Michel, L. Prejbenu-Buda, et al., Nat. Matter. **6**, 447 (2007).

[15] I. Firastrau, U. Ebels, L. Buda-Prejbeanu, J.-C. Toussaint, C. Thirion, and B. Dieny, J. Magn. Magn. Mater. **310**, 2029 (2007).

[16] U. Ebels, D. Houssameddine, I. Firastrau, D. Gusakova, C. Thirion, B. Dieny, and L. D. Buda-Prejbeanu, Phys. Rev. B **78**, 024436 (2008).

[17] T. J. Silva and M. W. Keller, IEEE Trans. Magn. **46**, 3555 (2010).

[18] H. Suto, T. Yang, T. Nagasawa, K. Kudo, K. Mizushima, and R. Sato, J. Appl. Phys. **112**, 083907 (2012).

[19] B. Lacoste, L. D. Buda-Prejbeanu, U. Ebels, and B. Dieny, Phys. Rev. B **88**, 054425 (2013).

[20] K. Kudo, H. Suto, T. Nagasawa, K. Mizushima, and R. Sato, J. Appl. Phys. **116**, 163911 (2014).

[21] S. Bosu, H. S-Amin, Y. Sakuraba, M. Hayashi, C. Abert, D. Suess, T. Schrefl, and K. Hono, Appl. Phys. Lett. **108**, 072403 (2016).

[22] M. Oogane, T. Wakitani, S. Yakata, R. Yilgin, Y. Ando, A. Sakuma, and T. Miyazaki, Jpn. J. Appl. Phys. **45**, 3889 (2006).

[23] S. Tsunegi, H. Kubota, S. Tamaru, K. Yakushiji, M. Konoto, A. Fukushima, T. Taniguchi, H. Arai, H. Imamura, and S. Yuasa, Appl. Phys. Express **7**, 033004 (2014).

[24] R. Hiramatsu, H. Kubota, S. Tsunegi, S. Tamaru, K. Yakushiji, A. Fukushima, R. Matsumoto, H. Imamura, and S. Yuasa (to be published).

[25] J. Z. Sun, Phys. Rev. B **62**, 570 (2000).

[26] J. Grollier, V. Cros, H. Jaffrés, A. Hamzic, J. M. George, G. Faini, J. B. Youssef, H. LeGall, and A. Fert, Phys. Rev. B **67**, 174402 (2003).

[27] H. Morise and S. Nakamura, Phys. Rev. B **71**, 014439 (2005).

[28] G. Bertotti, I. D. Mayergoyz, and C. Serpico, J. Appl. Phys. **95**, 6598 (2004).

[29] G. Bertotti, C. Serpico, I. D. Mayergoyz, A. Magni, M. d'Aquino, and R. Bonin, Phys. Rev. Lett. **94**, 127206 (2005).

[30] C. Serpico, M. d'Aquino, G. Bertotti, and I. D. Mayergoyz, J. Magn. Magn. Mater. **290**, 502 (2005).

[31] G. Bertotti, I. Mayergoyz, and C. Serpico, *Nonlinear Magnetization Dynamics in Nanosystems* (Elsevier, Oxford, 2009).

[32] D. M. Apalkov and P. B. Visscher, Phys. Rev. B **72**, 180405 (2005).

[33] B. Hillebrands and A. Thiaville, eds., *Spin Dynamics in Confined Magnetic Structures III*

(Springer, Berlin, 2006).

[34] Y. B. Bazaliy and F. Arammash, Phys. Rev. B **84**, 132404 (2011).

[35] M. Dykman, ed., *Fluctuating Nonlinear Oscillators* (Oxford University Press, Oxford, 2012), chap. 6.

[36] K. A. Newhall and E. V. Eijnden, J. Appl. Phys. **113**, 184105 (2013).

[37] T. Taniguchi, Y. Utsumi, M. Marthaler, D. S. Golubev, and H. Imamura, Phys. Rev. B **87**, 054406 (2013).

[38] T. Taniguchi, Phys. Rev. B **90**, 024424 (2014).

[39] T. Taniguchi, Phys. Rev. B **91**, 104406 (2015).

[40] D. Pinna, D. L. Stein, and A. D. Kent, Phys. Rev. B **90**, 174405 (2014).

[41] V. L. Safonov, J. Appl. Phys. **91**, 8653 (2002).

[42] S. Zhang and S. S.-L. Zhang, Phys. Rev. Lett. **102**, 086601 (2009).

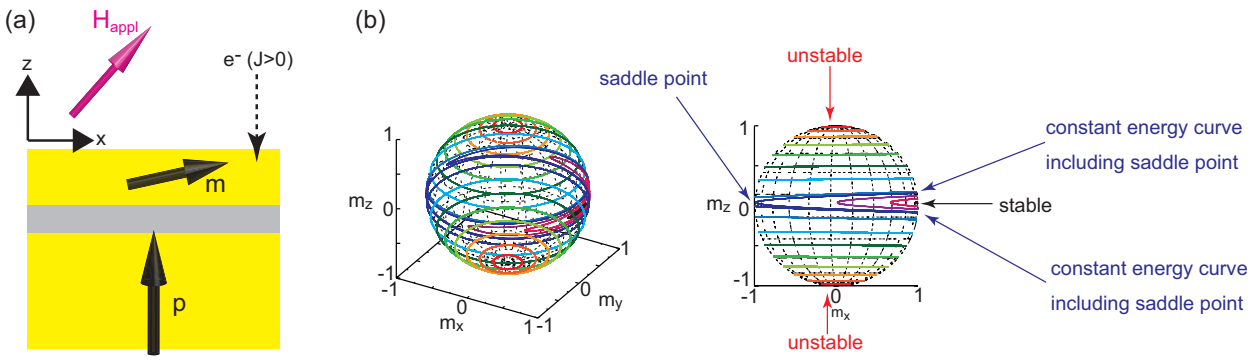

FIG. 1: (a) Schematic view of the system considered in this study. The unit vectors pointing in the magnetization direction of the free and pinned layers are denoted as **m** and **p**, respectively. The positive electric current corresponds to the electrons flowing from the free layer to the pinned layer. The external field lies in the xz plane. (b) Schematic views of the constant energy curves.

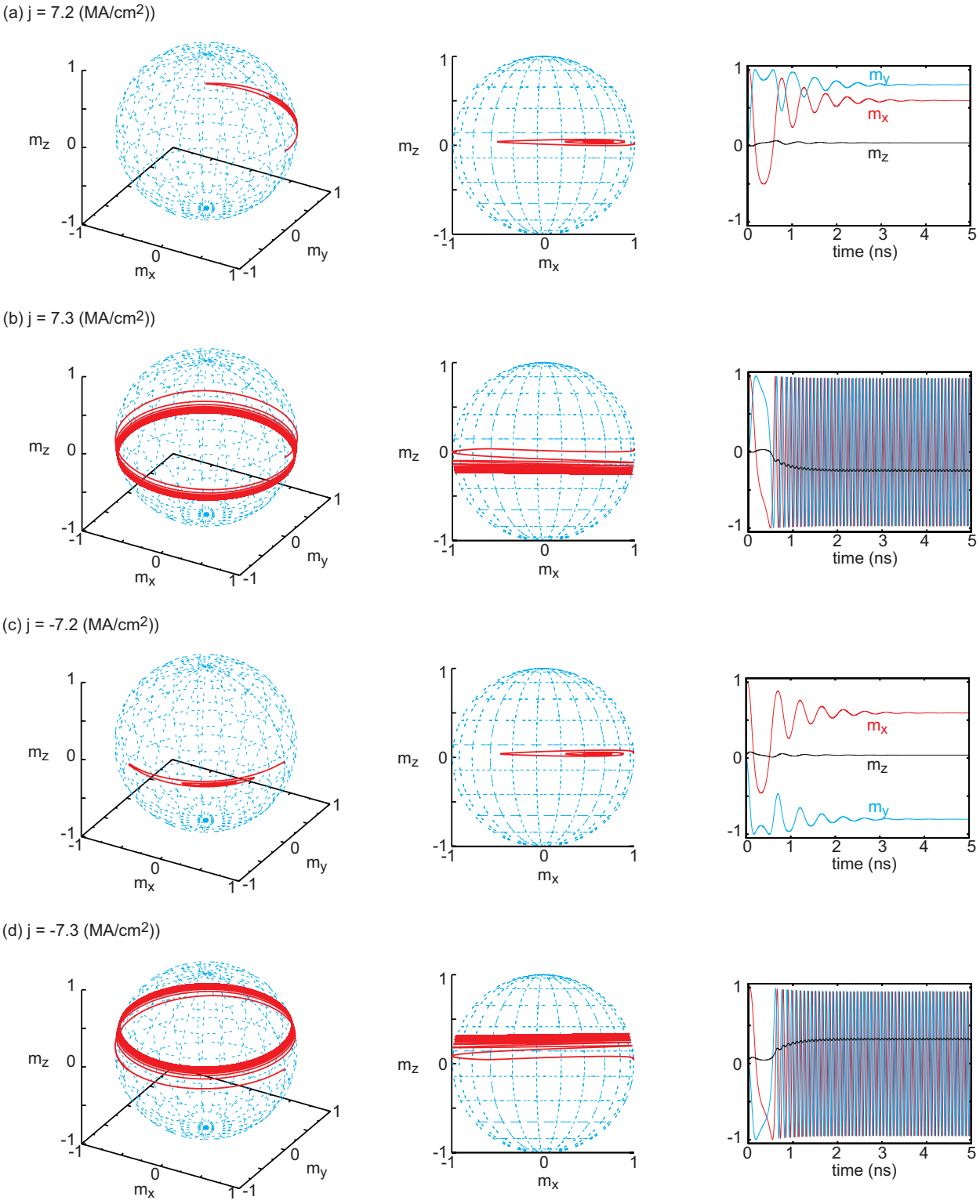

FIG. 2: The trajectories of the magnetization dynamics on the unit spheres. The time evolutions of the magnetization components are also shown. The values of the current density j are (a) 7.2, (b) 7.3, (c) -7.2, and (d) -7.3 $\times 10^6$ A/cm^2.

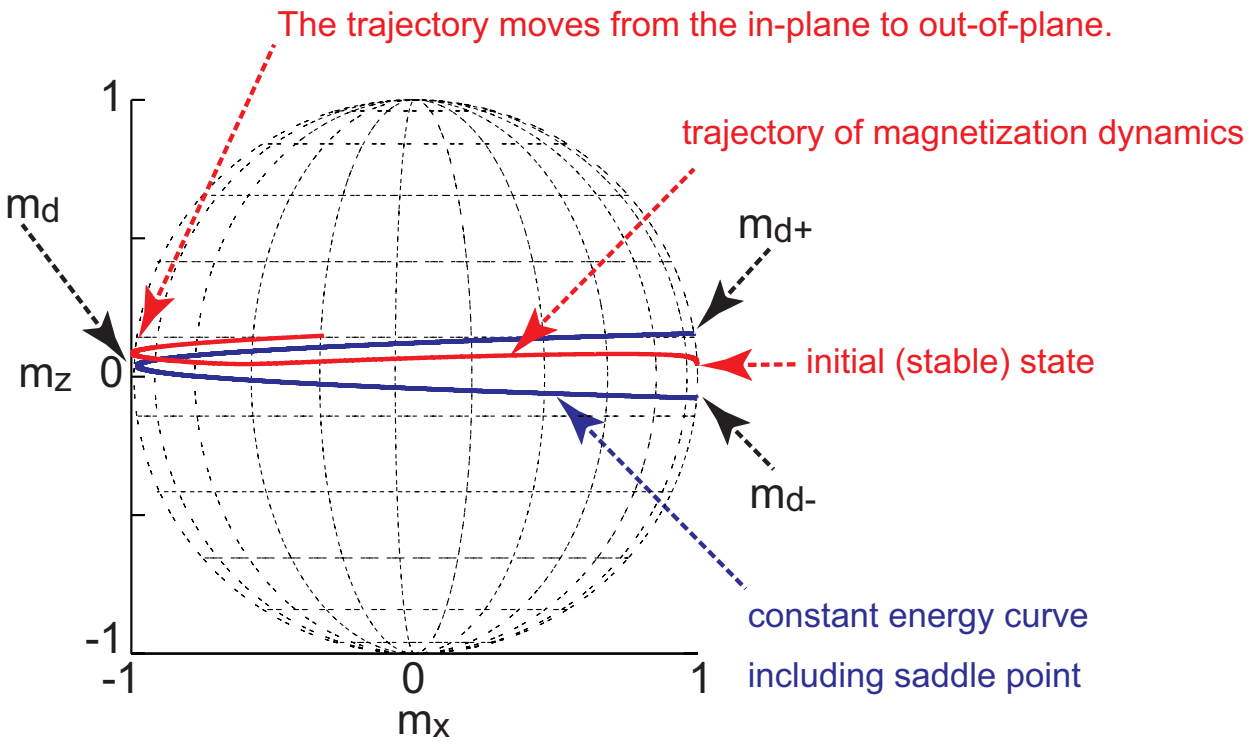

FIG. 3: The constant energy curve including the saddle point and the trajectory of the magnetization dynamics for $j = -7.3 \times 10^6$ A/cm^2. The point $\mathbf{m}_{\rm d}$ is the saddle point, while $\mathbf{m}_{\rm d\pm}$ are points on the constant energy curve of $E_{\rm saddle}$ and locating in the xz plane.

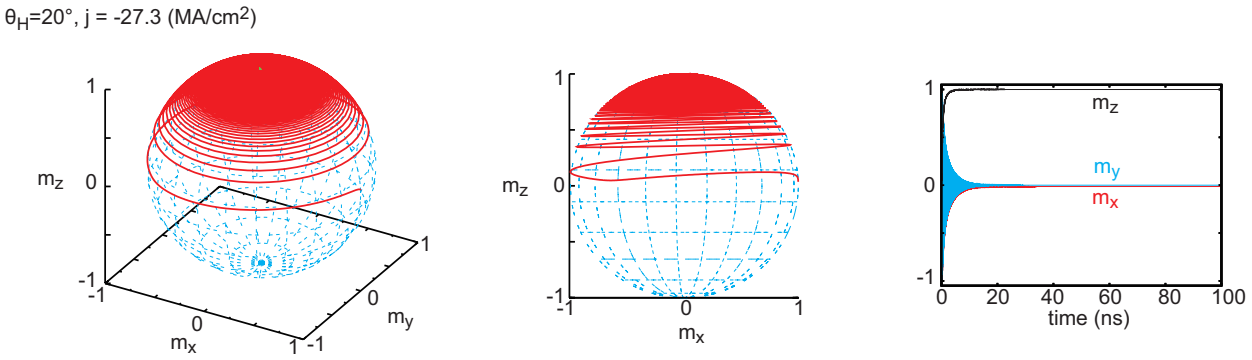

FIG. 4: The trajectories of the magnetization dynamics on the unit spheres and the time evolutions of the magnetization components for $\theta_H = 20^\circ$ and $j = -27.3 \times 10^6$ A/cm^2.

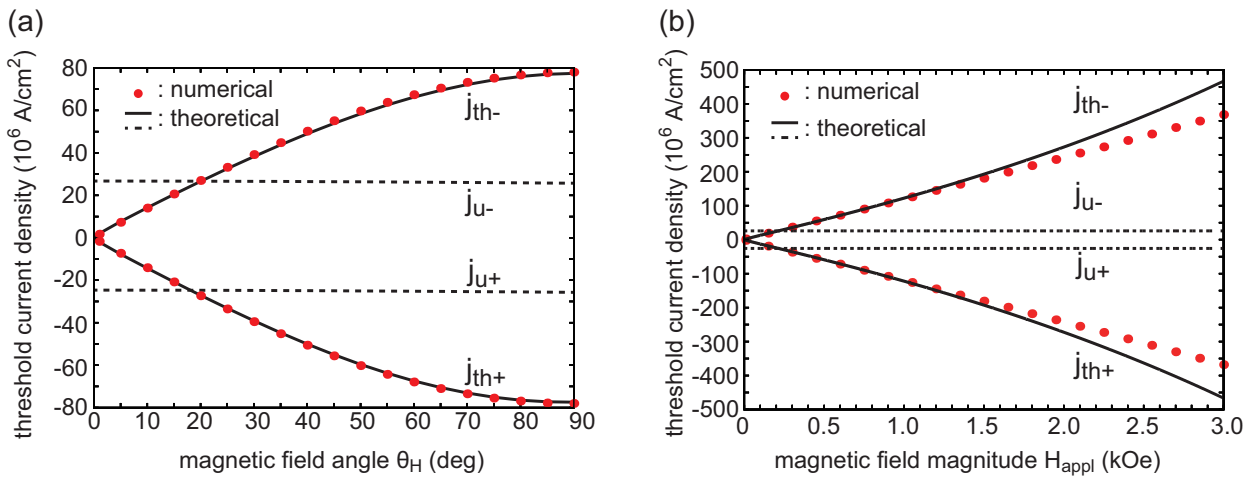

FIG. 5: Dependences of the threshold current densities estimated by numerically solving the LLG equation (1) (dots), the theoretical instability threshold $j_{\rm th\pm}$, Eq. (17), (solid lines), and the current densities $j_{\rm u\pm}$, Eq. (32), (dotted lines) on (a) the applied field angle θ_H ($H_{\rm appl} = 650$ Oe) and (b) the magnitude $H_{\rm appl}$ ($\theta_H = 90^\circ$).

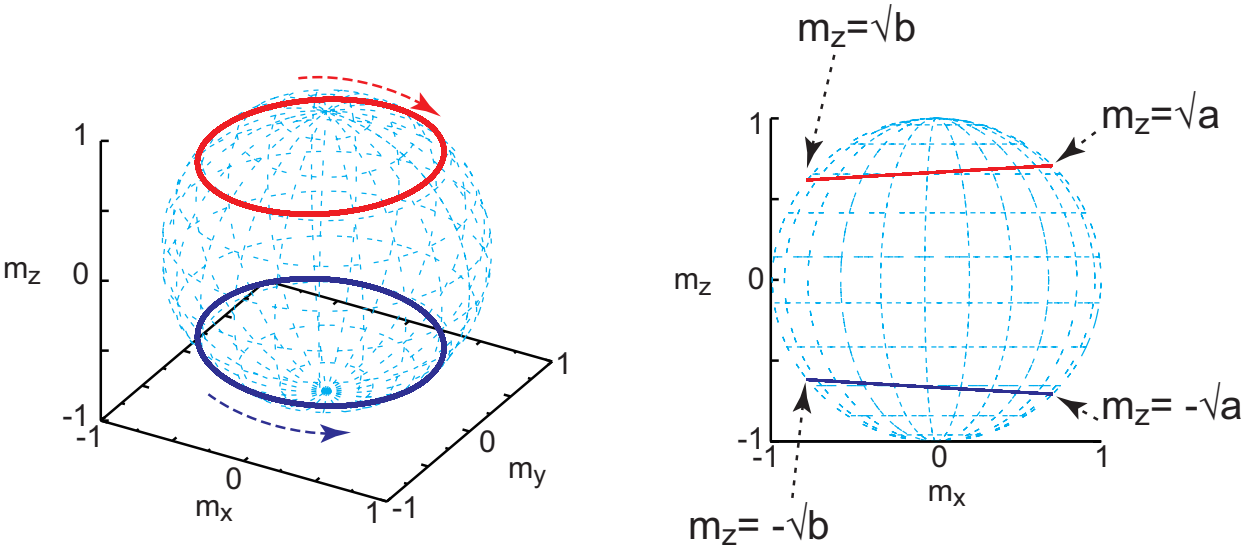

FIG. 6: The examples of the out-of-plane precession trajectories (constant energy curves), where the arrows indicate the precession directions. The constant energy curves cross the xz plane at $m_z = \pm\sqrt{a}, \pm\sqrt{b}$.